Exchange-Correlation Thermal Effects in Shocked Deuterium: Softening the Principal Hugoniot and Thermophysical Properties

V. V. Karasiev, S. X. Hu, M. Zaghoo, and T. R. Boehly

Laboratory for Laser Energetics, University of Rochester

Reliably predicting the properties of hydrogen and its isotopes under extreme conditions remains a problem of great importance and broad scientific interest. Accurate knowledge of the equation of state (EOS) and transport properties over a wide range of thermodynamic conditions of this simplest and most-abundant element in the universe is used as input for planetary astrophysics models to describe interiors of planets[1] as well as the inertial confinement fusion (ICF) simulations to design targets.[2–4] The most-advanced theoretical and computational methods are used to interpret experimental results and to predict properties at thermodynamic conditions that are difficult to access experimentally.

On the other hand, new experimental measurements with improved accuracy[5,6] serve as an important benchmark to assess the accuracy of theoretical predictions. It was found[6] that recent shock-compression data for deuterium are well described by finite-temperature density functional theory (DFT) methods.[7–9] Standard generalized gradient approximation (GGA) exchange-correlation (XC) functionals such as Perdew–Burke–Ernzerhof (PBE)[10] describe the peak compression reasonably well, but at pressures above 250 GPa along the Hugoniot, the DFT calculations with the PBE functional predict a stiffer behavior than recent experimental data.[5]

All current DFT calculations of the Hugoniot data and transport coefficients are performed with temperature-independent XC functionals developed for ground state;[4,6,11–14] therefore, XC thermal effects, which play an important role in warm-dense-matter (WDM) conditions,[15] are not taken into account. Figure 1 shows the (r_s,t) domain where the temperature dependence of XC might be important for accurate predictions. The relative importance of XC thermal effects is shown as a function of the Wigner–Seitz radius $r_s = (3/4\pi n)^{1/3}$ and reduced temperature $t = T/T_F$, where $T_F = (3\pi^2 n)^{2/3}/2k_B$ is the Fermi temperature and n is the electron number density. XC thermal effects might become important for t values around a few tenths and above. Here we

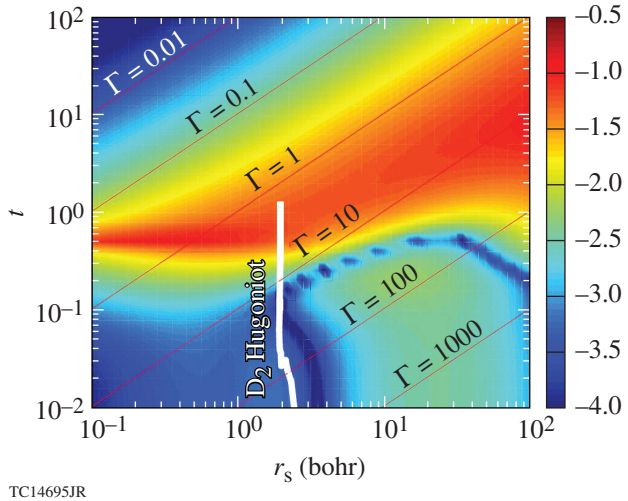

TC14695JR

Figure 1

The relative importance of explicit temperature dependence in the XC free-energy functional for the homogeneous electron gas measured as $\log_{10}\left\{\left|f_{xc}(r_s,t)-e_{xc}(r_s)\right|/\left[\left|f_s(r_s,t)\right|+\left|e_{xc}(r_s)\right|\right]\right\}$, where f_{xc} is the XC free-energy per particle given by the corrKSDT parameterization,[16,17] e_{xc} is the zero-temperature XC energy per particle,[18] and f_s is the noninteracting free energy per particle.[19] $\Gamma = 2\lambda^2 r_s/t$ with $\lambda = (4/9\pi)^{1/3}$ is the classical coupling parameter. The solid white line corresponds to the liquid deuterium principal Hugoniot path; the end point corresponds to $P = 1$ TPa.

focus on the study of the optical and transport properties along the principal Hugoniot of deuterium with a temperature-dependent Karasiev–Dufty–Trickey (KDT16) generalized gradient approximation XC functional.[16]

Figure 2 compares our theoretical predictions and experimental results across the molecular-to-atomic (MA) transition (low-pressure range $P < 150$ GPa) (Ref. 6). Both functionals, KDT16 and PBE, are in good agreement with experimental measurements in the range of pressure up to 200 GPa. At higher pressures, however, the PBE curve becomes noticeably stiffer as compared to the recent experimental data;[5] the disagreement reaches about 4% at $P = 550$ GPa. The KDT16 predicts a curve that is softer by slightly more than 1% beyond 250 GPa as compared to PBE. Increasing the simulation cell size from 64 to 128 atoms in this range of pressure leads to further softening of the Hugoniot. The KDT16 compressibility is within the experimental uncertainty in the entire pressure range (including high pressures $P > 250$ GPa). Therefore, the inclusion of XC thermal effects in calculations makes the deuterium Hugoniot softer at $P > 250$ GPa and improves agreement with the experimental data; the KDT16 XC functional is able to describe the principal Hugoniot of liquid deuterium consistently over the entire pressure range.

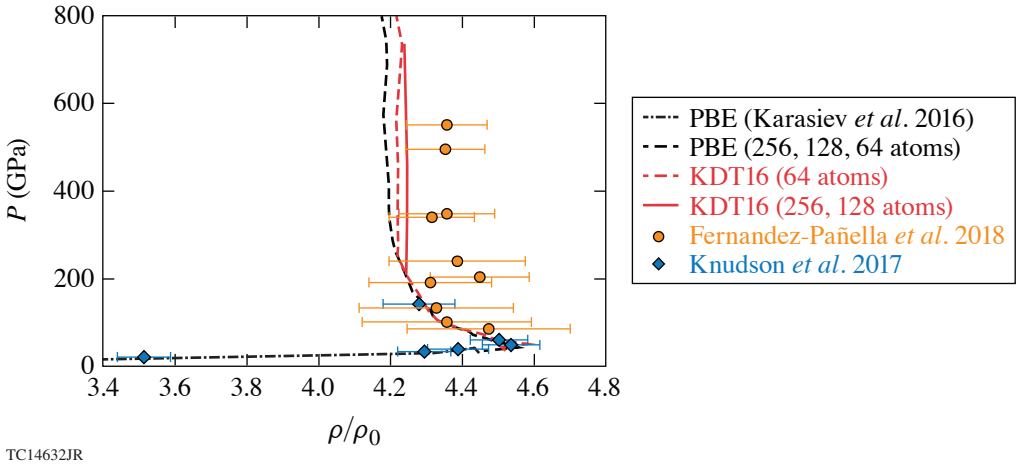

Figure 2
Deuterium principal Hugoniot derived from the initial state $\rho_0 = 0.172$ g/cm^3 and $T_0 = 20$ K. The PBE (dashed black) and KDT16 (dashed red) curves are obtained by combining results from simulations with 256 atoms ($6 \le T \le 20$ kK, pressure range between 34 and 86 GPa for both functionals), 128 atoms ($25 \le T \le 50$ kK, pressure range between 104 and 208 GPa for KDT16), 64 atoms ($60 \le T \le 150$ kK, pressure range between 253 and 736 GPa for KDT16), and 32 atoms for $T = 200$ kK. The solid red curve corresponds to the KDT16 results from simulations with 256 atoms ($6 \le T \le 20$ kK) and 128 atoms ($25 \le T \le 150$ kK).

The reflectivity along the deuterium Hugoniot was calculated at 532 and 808 nm with the KDT16 XC functional and our predicted value of the refractive index. Results of recent experiments[20] on OMEGA and previous measurements[21] are shown in Fig. 3. There is excellent agreement between the KDT16 values and experimental data at 808-nm wavelength for the range of shock speeds considered in calculations, even though the experimental data have relatively large error bars. The KDT16 results at 532 nm are in very good agreement with recent OMEGA experimental data for shock speeds below 50 km/s. The reflectivity is underestimated by the DFT calculations at high shock speeds $U_s > 50$ km/s as compared to the experiment. Experimental reflectance as a function of shock speed changes the slope at U_s near 45 km/s ($T \approx 0.4\ T_F = 60$ kK); this change in the slope is related to lifting of the Fermi degeneracy. The system starts to behave as a classical one at a significantly lower temperature as compared to T_F (see details in Ref. 20). Calculated KDT16 reflectivity at the same 532-nm wavelength rises very quickly from 0.29 at 16 km/s ($T \approx 6$ kK) to 0.39 at 20 km/s ($T \approx 12$ kK), which roughly corresponds to maximum compression near molecular-to-atomic transition; it slowly continues to increase and near 43 km/s the slope also increases.

The deuterium system along the Hugoniot experiences transformations from an insulating molecular liquid to atomic poor metallic liquid and finally to nondegenerate classical plasma. The signature of the molecular-to-atomic transition is found in a sharp increase of electrical dc conductivity and reflectivity at shock speeds in the range between 16 and 20 km/s (a range of temperature

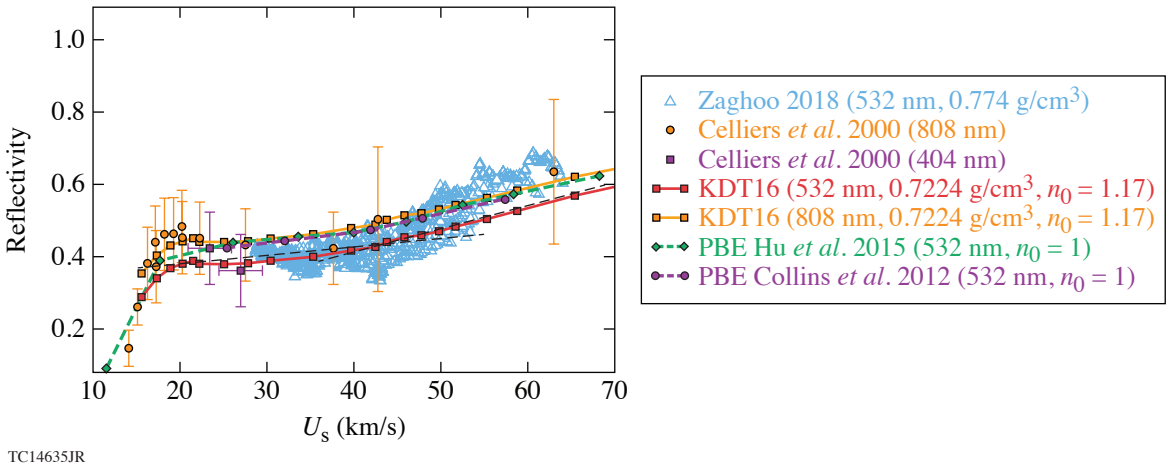

Figure 3
Reflectivity of shocked deuterium. Theoretical DFT predictions and experimental data are compared.

between 6 and 12 kK). An increase in the slope of calculated reflectivity at $U_s \approx 43$ km/s ($T \approx 0.4\ T_F = 60$ kK), related to the breakdown of the electrons' degeneracy and emergence of classical statistics,[20] is in agreement with experimental measurements.

Our results confirm that the crossover between the quantum and classical statistics occurs below the $T = T_F$ limit. This is apparent in the observed change in the transport and the thermodynamic properties of the deuterium fluid in the region of 0.4 to 0.65 T_F. Future work should investigate the dependence of the onset of this crossover on density.

This material is based upon work supported by the Department of Energy National Nuclear Security Administration under Award Number DE-NA0003856 and U.S. National Science Foundation PHY Grant No. 1802964.

1. J. J. Fortney and N. Nettelmann, Space Sci. Rev. **152**, 423 (2010).
2. S. X. Hu *et al*., Phys. Rev. B **84**, 224109 (2011).
3. S. X. Hu *et al*., Phys. Rev. E **90**, 033111 (2014).
4. S. X. Hu *et al*., Phys. Plasmas **22**, 056304 (2015).
5. A. Fernandez-Pañella *et al*., "Shock Compression of Liquid Deuterium up to 1 TPa," to be published in Physical Review Letters.
6. M. D. Knudson and M. P. Desjarlais, Phys. Rev. Lett. **118**, 035501 (2017).
7. N. D. Mermin, Phys. Rev. **137**, A1441 (1965).
8. M. V. Stoitsov and I. Zh. Petkov, Ann. Phys. **184**, 121 (1988).
9. R. M. Dreizler, in *The Nuclear Equation of State. Part A: Discovery of Nuclear Shock Waves and the EOS*, edited by W. Greiner and H. Stöcker, Nato Science Series B (1989), pp. 521–532.
10. J. P. Perdew, K. Burke, and M. Ernzerhof, Phys. Rev. Lett. **77**, 3865 (1996); **78**, 1396(E) (1997).
11. B. Holst, R. Redmer, and M. P. Desjarlais, Phys. Rev. B **77**, 184201 (2008).
12. L. Caillabet, S. Mazevet, and P. Loubeyre, Phys. Rev. B **83**, 094101 (2011).
13. L. A. Collins *et al*., Phys. Rev. B **63**, 184110 (2001).
14. L. A. Collins, J. D. Kress, and D. E. Hanson, Phys. Rev. B **85**, 233101 (2012).

15. V. V. Karasiev, L. Calderín, and S. B. Trickey, Phys. Rev. E **93**, 063207 (2016).

16. V. V. Karasiev, J. W. Dufty, and S. B. Trickey, Phys. Rev. Lett. **120**, 076401 (2018).

17. V. V. Karasiev *et al*., Phys. Rev. Lett. **112**, 076403 (2014).

18. J. P. Perdew and A Zunger, Phys. Rev. B **23**, 5048 (1981).

19. R. P. Feynman, N. Metropolis, and E. Teller, Phys. Rev. **75**, 1561 (1949).

20. M. Zaghoo *et al*., Phys. Rev. Lett. **122**, 085001 (2019).

21. P. M. Celliers *et al*., Phys. Rev. Lett. **84**, 5564 (2000).